haler, Eds., vol. 16 of *Lecture Notes in Earth Sciences* (Springer-Verlag, New York, 1988), pp. 83–116.
30. N. J. Shackleton, *Quat. Sci. Rev.* **6**, 183 (1987).
31. T. J. Crowley and R. K. Matthews, *Geology* **11**, 275 (1983).
32. Critical age ^{230}Th determinations for MIS 5e are 116 ± 0.9 ka for the end and 128 ± 1 ka for the beginning (*35*); these have been plotted at a nominal +6 m (*36*). A point at −60 m at 132 ± 2 ka represents the coral at "Aladdin's Cave" (*37*). Reliable (supported by ^{231}Pa data) ages for MIS 5a (82.8 ± 1.0 ka) and MIS 5c (104.2 ± 1.2 ka) are from Barbados (*36, 38*). Sea levels during MIS 3 are from the Huon Peninsula, New Guinea (*39*), and the plotted points for the most recent deglaciation are from offshore Barbados (*40*).
33. The amplitude of the 100-ky component in ice volume variability may be even smaller if an account is taken of the effect of changing atmospheric CO_2 pressure (P_{CO_2}) on $\delta^{18}O$ fractionation in the stratosphere (*11*). As suggested in (*11*), the magnitude of this effect is of the order of 0.4‰ for today's atmospheric P_{CO_2}, equating to an effect of the order of 0.13‰ per 100-ppmv change in P_{CO_2}. Because the coherent amplitude of the P_{CO_2} signal at 100 ky is 36 ppmv (Table 2), this correction will reduce the true amplitude of the 100-ky ice volume signal by ~0.047‰ (from 0.28 to 0.23‰). Supplementary material (*17*) illustrates the effect of making this correction.
34. J. Imbrie, *J. Geol. Soc. London* **142**, 417 (1985).
35. C. H. Stirling, T. M. Esat, K. Lambeck, M. T. McCulloch, *Earth Planet. Sci. Lett.* **160**, 745 (1998)
36. R. K. Matthews, *Quat. Res.* **3**, 147 (1973)
37. T. M. Esat, M. T. McCulloch, J. Chappell, B. Pillans, A. Omura, *Science* **283**, 197 (1999).
38. R. L. Edwards, H. Cheng, M. T. Murrell, S. J. Goldstein, *Science* **276**, 782 (1997).
39. J. Chappell *et al.*, *Earth Planet. Sci. Lett.* **141**, 227 (1996).
40. E. Bard, B. Hamelin, R. G. Fairbanks, A. Zindler, *Nature* **345**, 405 (1990).
41. Because the orbital records are not sinusoidal, the estimate of coherent amplitude is not readily used; therefore, tuning targets were created with the same coherent amplitudes empirically. In the precession band, the value given as coherent amplitude is ~38% of the maximum high-to-low range (which occurs between 209 and 220 ky); in the obliquity band, it is ~54% of the maximum high-to-low range (between 212 and 232 ky).
42. This work was supported by UK Natural Environment Research Council grant GR3/12889. I am very grateful to S. Crowhurst for considerable assistance in data manipulation. I was inspired to tackle the data discussed here by discussions with M. Bender and, more recently, with D. Raynaud. The final manuscript was considerably improved as a consequence of reviews by M. Bender, J. Imbrie, and two anonymous reviewers.

17 May 2000; accepted 31 July 2000

Bacterial Rhodopsin: Evidence for a New Type of Phototrophy in the Sea

Oded Béjà,[1] L. Aravind,[2] Eugene V. Koonin,[2] Marcelino T. Suzuki,[1] Andrew Hadd,[3] Linh P. Nguyen,[3] Stevan B. Jovanovich,[3] Christian M. Gates,[3] Robert A. Feldman,[3] John L. Spudich,[4] Elena N. Spudich,[4] Edward F. DeLong[1]*

Extremely halophilic archaea contain retinal-binding integral membrane proteins called bacteriorhodopsins that function as light-driven proton pumps. So far, bacteriorhodopsins capable of generating a chemiosmotic membrane potential in response to light have been demonstrated only in halophilic archaea. We describe here a type of rhodopsin derived from bacteria that was discovered through genomic analyses of naturally occuring marine bacterioplankton. The bacterial rhodopsin was encoded in the genome of an uncultivated γ-proteobacterium and shared highest amino acid sequence similarity with archaeal rhodopsins. The protein was functionally expressed in *Escherichia coli* and bound retinal to form an active, light-driven proton pump. The new rhodopsin exhibited a photochemical reaction cycle with intermediates and kinetics characteristic of archaeal proton-pumping rhodopsins. Our results demonstrate that archaeal-like rhodopsins are broadly distributed among different taxa, including members of the domain *Bacteria*. Our data also indicate that a previously unsuspected mode of bacterially mediated light-driven energy generation may commonly occur in oceanic surface waters worldwide.

Retinal (vitamin A aldehyde) is a chromophore that binds integral membrane proteins (opsins) to form light-absorbing pigments called rhodopsins. Rhodopsins are currently known to belong to two distinct protein families. The visual rhodopsins, found in eyes throughout the animal kingdom (*1*), are photosensory pigments. Archaeal rhodopsins, found in extreme halophiles, function as light-driven proton pumps (bacteriorhodopsins), chloride ion pumps (halorhodopsins), or photosensory receptors (sensory rhodopsins) (*2–5*). The two protein families show no significant sequence similarity and may have different origins. They do, however, share identical topologies characterized by seven transmembrane α-helices that form a pocket in which retinal is covalently linked, as a protonated Schiff base, to a lysine in the seventh transmembrane helix (helix G). Recently, a protein with high sequence similarity to the archaeal rhodopsins has also been found in the eukaryote *Neurospora crassa* (*6*). The eucaryal rhodopsin formed a photochemically reactive pigment when bound to all-*trans* retinal and exhibited photocycle kinetics similar to those of archaeal sensory rhodopsins (*7*). To date, however, no rhodopsin-like sequences have been reported in members of the domain *Bacteria*.

Cloning of proteorhodopsin. Sequence analysis of a 130-kb genomic fragment that encoded the ribosomal RNA (rRNA) operon from an uncultivated member of the marine γ-*Proteobacteria* (that is, the "SAR86" group) (*8, 9*) (Fig. 1A) also revealed an open reading frame (ORF) encoding a putative rhodopsin (referred to here as proteorhodopsin) (*10*). The inferred amino acid sequence of the proteorhodopsin showed statistically significant similarity to archaeal rhodopsins (*11*). The majority of predicted proteins encoded by ORFs upstream and downstream of the proteorhodopsin gene, as well as the rRNA operon, showed highest similarity to proteobacterial homologs. Given the large amount of apparent lateral gene transfer observed in recent whole genome studies, it is not surprising that some predicted proteins (17 of 74) had significantly greater similarity to those from other bacterial groups, including *Actinomycetes* and Gram-positive bacteria (*12, 13*). No other ORFs encoding archaeal-like genes, however, were detected in the vicinity of the proteorhodopsin gene, verifying the bacterial origin of the 130-kb genome fragment.

The proteorhodopsin gene encoded a polypeptide of 249 amino acids, with a molecular weight of 27 kD. Hydropathy plots indicated seven transmembrane domains, a typical feature of the rhodopsin protein family, that aligned well with the corresponding helices of the archaeal rhodopsins. The amino acid residues that form a retinal binding pocket in archaeal rhodopsins are also highly conserved in proteorhodopsin (Fig. 2). In particular, the critical lysine residue in helix G, which forms the Schiff base linkage with retinal in archaeal rhodopsins, is present in proteorhodopsin. Analysis of a structural model of proteorhodopsin (*14*), in conjunc-

[1]Monterey Bay Aquarium Research Institute, Moss Landing, CA 95039–0628, USA. [2]National Center for Biotechnology Information, National Library of Medicine, National Institutes of Health, Bethesda, MD 20894, USA. [3]Molecular Dynamics, Amersham Pharmacia Biotech, Sunnyvale, CA 94086, USA. [4]Department of Microbiology and Molecular Genetics, The University of Texas Medical School, Houston, TX 77030, USA.

*To whom correspondence should be addressed. E-mail: delong@mbari.org.

tion with multiple sequence alignments, indicates that the majority of active site residues are well conserved between proteorhodopsin and archaeal bacteriorhodopsins (*15*).

A phylogenetic comparison with archaeal rhodopsins placed proteorhodopsin on an independent long branch, with moderate statistical support for an affiliation with sensory rhodopsins (*16*) (Fig. 1B). The finding of archaeal-like rhodopsins in organisms as diverse as marine proteobacteria and eukarya (*6*) suggests a potential role for lateral gene transfer in their dissemination. Available genome sequence data are insufficient to identify the evolutionary origins of the proteorhodopsin genes. The environments from which the archaeal and bacterial rhodopsins originate are, however, strikingly different. Proteorhodopsin is of marine origin, whereas the archaeal rhodopsins of extreme halophiles experience salinity 4 to 10 times greater than that in the sea (*14*).

Functional analysis. To determine whether proteorhodopsin binds retinal, we expressed the protein in *Escherichia coli* (*17*). After 3 hours of induction in the presence of retinal, cells expressing the protein acquired a reddish pigmentation (Fig. 3A). When retinal was added to the membranes of cells expressing the proteorhodopsin apoprotein, an absorbance peak at 520 nm was observed after 10 min of incubation (Fig. 3B). On further incubation, the peak at 520 nm increased and had a ~100-nm half-bandwidth. The 520-nm pigment was generated only in membranes containing proteorhodopsin apoprotein, and only in the presence of retinal, and its ~100-nm half-bandwidth is typical of retinylidene protein absorption spectra found in other rhodopsins. The red-shifted λ_{max} of retinal (λ_{max} = 370 nm in the free state) is indicative of a protonated Schiff base linkage of the retinal, presumably to the lysine residue in helix G (*18*).

Light-mediated proton translocation was determined by measuring pH changes in a cell suspension exposed to light. Net outward transport of protons was observed solely in proteorhodopsin-containing *E. coli* cells and only in the presence of retinal and light (Fig. 4A). Light-induced acidification of the medium was completely abolished by the presence of a 10 μM concentration of the protonophore carbonyl cyanide m-chlorophenylhydrazone (*19*). Illumination generated a membrane electrical potential in proteorhodopsin-containing right-side-out membrane vesicles, in the presence of retinal, reaching –90 mV 2 min after light onset (*20*) (Fig. 4B). These data indicate that proteorhodopsin translocates protons and is capable of generating membrane potential in a physiologically relevant range. Because these activities were observed in *E. coli* membranes containing overexpressed protein, the levels of proteorhodopsin activity in its native state remain to be determined. The ability of proteorhodopsin to generate a physiologically significant membrane potential, however, even when heterologously expressed in nonnative membranes, is consistent with a postulated proton-pumping function for proteorhodopsin.

Archaeal bacteriorhodopsin, and to a lesser extent sensory rhodopsins (*21*), can both mediate light-driven proton-pumping activity. However, sensory rhodopsins are generally cotranscribed with genes encoding their own transducer of light stimuli [for example, Htr (*22*, *23*)]. Although sequence analysis of proteorhodopsin shows moderate statistical support for a specific relationship with sensory rhodopsins, there is no gene for an Htr-like regulator adjacent to the proteorhodopsin gene. The absence of an Htr-like gene in close proximity to the proteorhodopsin gene suggests that proteorhodopsin may function primarily as a light-driven proton pump. It is possible, however, that such a regulator might be encoded elsewhere in the proteobacterial genome.

To further verify a proton-pumping function for proteorhodopsin, we characterized the kinetics of its photochemical reaction cycle. The transport rhodopsins (bacteriorhodopsins and halorhodopsins) are characterized by cyclic photochemical reaction se-

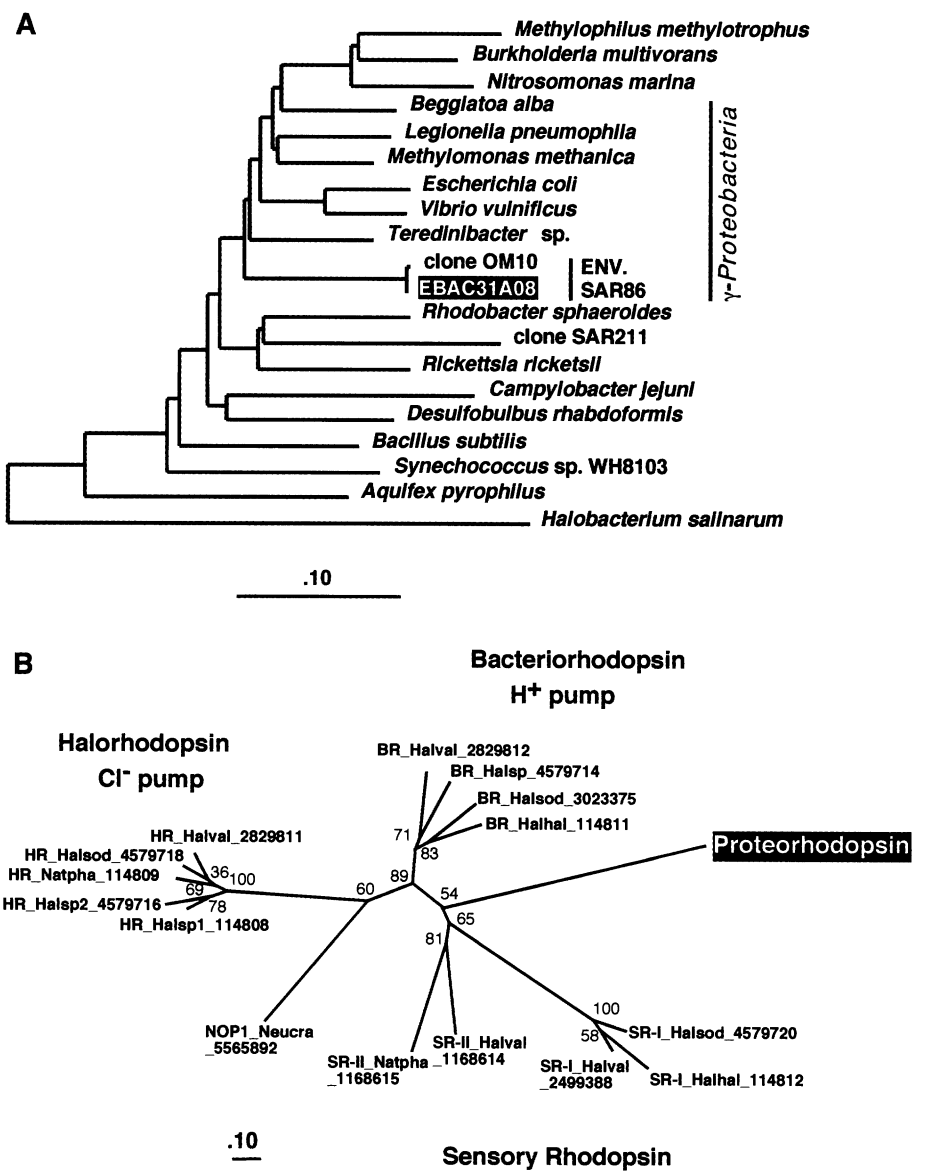

Fig. 1. (**A**) Phylogenetic tree of bacterial 16*S* rRNA gene sequences, including that encoded on the 130-kb bacterioplankton BAC clone (EBAC31A08) (*16*). (**B**) Phylogenetic analysis of proteorhodopsin with archaeal (BR, HR, and SR prefixes) and *Neurospora crassa* (NOP1 prefix) rhodopsins (*16*). Nomenclature: Name_Species.abbreviation_Genbank.gi (HR, halorhodopsin; SR, sensory rhodopsin; BR, bacteriorhodopsin). Halsod, *Halorubrum sodomense*; Halhal, *Halobacterium salinarum* (*halobium*); Halval, *Haloarcula vallismortis*; Natpha, *Natronomonas pharaonis*; Halsp, *Halobacterium* sp; Neucra, *Neurospora crassa*.

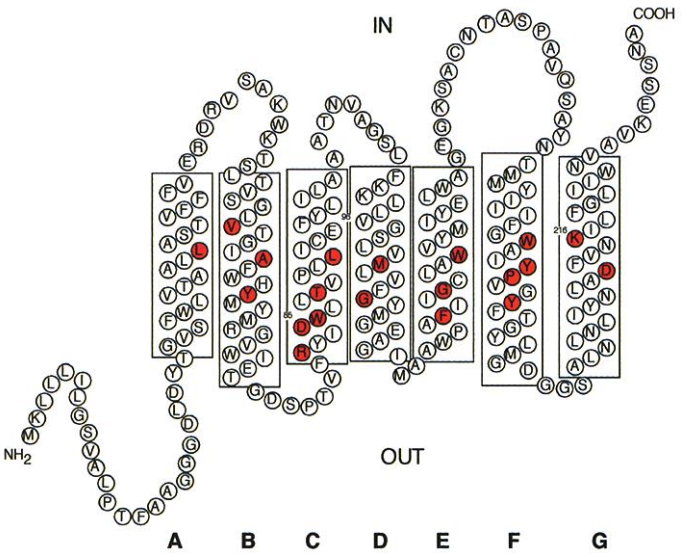

Fig. 2. Secondary structure of proteorhodopsin. Single-letter amino acid codes are used (*33*), and the numbering is as in bacteriorhodopsin. Predicted retinal binding pocket residues are marked in red.

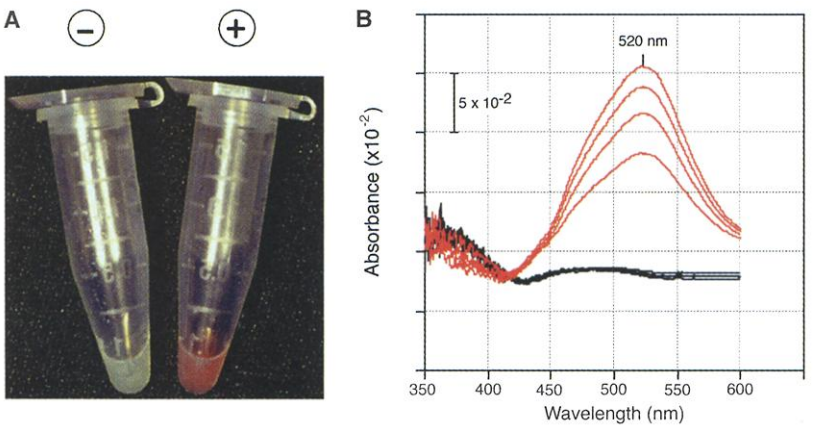

Fig. 3. (**A**) Proteorhodopsin-expressing *E. coli* cell suspension (+) compared to control cells (−), both with all-*trans* retinal. (**B**) Absorption spectra of retinal-reconstituted proteorhodopsin in *E. coli* membranes (*17*). A time series of spectra is shown for reconstituted proteorhodopsin membranes (red) and a negative control (black). Time points for spectra after retinal addition, progressing from low to high absorbance values, are 10, 20, 30, and 40 min.

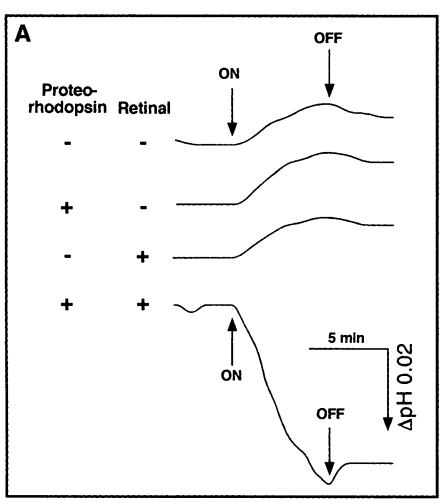

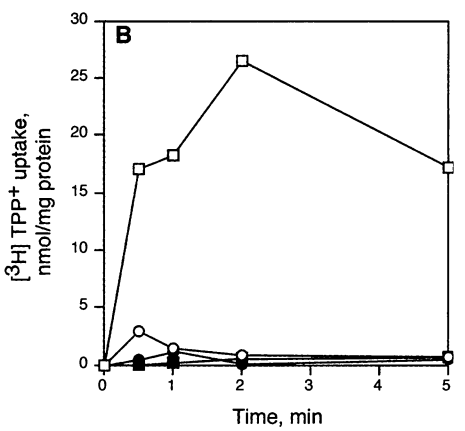

Fig. 4. (**A**) Light-driven transport of protons by a proteorhodopsin-expressing *E. coli* cell suspension. The beginning and cessation of illumination (with yellow light >485 nm) is indicated by arrows labeled ON and OFF, respectively. The cells were suspended in 10 mM NaCl, 10 mM $MgSO_4 \cdot 7H_2O$, and 100 μM $CaCl_2$. (**B**) Transport of $^3H^+$-labeled tetraphenylphosphonium ($[^3H^+]$TPP) in *E. coli* right-side-out vesicles containing expressed proteorhodopsin, reconstituted with (squares) or without (circles) 10 μM retinal in the presence of light (open symbols) or in the dark (solid symbols) (*20*).

quences (photocycles) that are typically <20 ms, whereas sensory rhodopsins are slow-cycling pigments with photocycle half-times >300 ms (*3*). This large kinetic difference is functionally important, because a rapid photocycling rate is advantageous for efficient ion pumping, whereas a slower cycle provides more efficient light detection because signaling states persist for longer times. To assess the photochemical reactivity of proteorhodopsin and its kinetics, we subjected membranes containing the pigment to a 532-nm laser flash and analyzed flash-induced absorption changes in the 50-μs to 10-s time window. We observed transient flash-induced absorption changes in the early times in this range (Fig. 5). Transient depletion occurred near the absorption maximum of the pigment (500-nm trace, Fig. 5, top panel), and transient absorption increase was detected at 400 nm and 590 nm, indicating a functional photocyclic reaction pathway. The absorption difference spectrum shows that within 0.5 ms, an intermediate with maximal absorption near 400 nm is produced (Fig. 5, bottom panel), which is typical of unprotonated Schiff base forms (M intermediates) of retinylidene pigments. The 5-ms minus 0.5-ms difference spectrum shows that after M decay, an intermediate species that is red-shifted from the unphotolyzed 520-nm state appears, which is analogous to the final intermediate (O) in bacteriorhodopsin. The decay of proteorhodopsin O is the rate-limiting step in the photocycle and is fit well by a single exponential process of 15 ms, with an upward baseline shift of 13% of the initial amplitude. A possible explanation is heterogeneity in the proteorhodopsin population, with 87% of the molecules exhibiting a 15-ms photocycle and 13% exhibiting a slower recovery. An alternative explanation is that photocycle complexity such as branching produces a biphasic O decay. Consistent with this alternative, the O recovery is fit equally well as a two-exponential process with a fast component, with a 9-ms half-time (61% of the total amplitude) and a slow component with a 45-ms half-time (39% of the total amplitude). In either case, the rapid photocycle rate, which is a distinguishing characteristic of ion pumps, provides additional strong evidence that proteorhodopsin functions as a transporter rather than as a sensory rhodopsin.

Implications. The γ-proteobacteria that harbor the proteorhodopsin are widely distributed in the marine environment. These bacteria have been frequently detected in culture-independent surveys (*24*) in coastal and oceanic regions of the Atlantic and Pacific Oceans, as well as in the Mediterranean Sea (*8*, *25*–*29*). In addition to its widespread distribution, preliminary data also suggest that this γ-proteobacterial group is abundant (*30*,

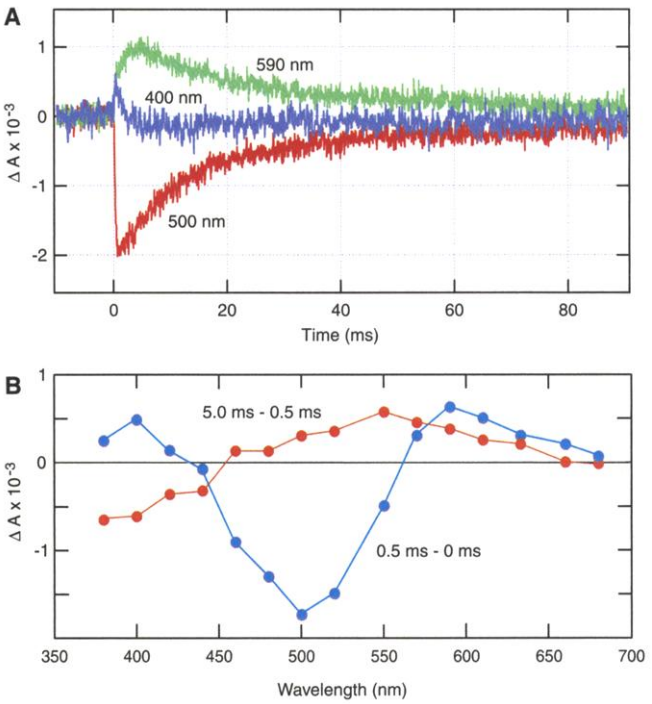

Fig. 5. Laser flash-induced absorbance changes in suspensions of *E. coli* membranes containing proteorhodopsin. A 532-nm pulse (6 ns duration, 40 mJ) was delivered at time 0, and absorption changes were monitored at various wavelengths in the visible range in a lab-constructed flash photolysis system as described (*34*). Sixty-four transients were collected for each wavelength. (**A**) Transients at the three wavelengths exhibiting maximal amplitudes. (**B**) Absorption difference spectra calculated from amplitudes at 0.5 ms (blue) and between 0.5 ms and 5.0 ms (red).

31) and specifically localized in marine surface waters. Preliminary data (*30*) also indicate that the abundance of SAR86-like bacteria positively correlates with proteorhodopsin mRNA expression. The absorbance λ_{max} of proteorhodopsin at 520 nm matches well with the photosynthetically available irradiance in the ocean's upper water column. Furthermore, some phylogenetic relatives of the proteorhodopsin-containing bacteria are chemolithoautotrophs that use CO_2 as a sole carbon source (*32*). Proteorhodopsin could support a photoheterotrophic lifestyle, or it might in fact support a previously unrecognized type of photoautotrophy in the sea. Either of these alternatives suggests the possibility of a previously unrecognized phototrophic pathway that may influence the flux of carbon and energy in the ocean's photic zone worldwide.

References and Notes

1. J. M. Baldwin, G. F. Schertler, V. M. Unger, *J. Mol. Biol.* **272**, 144 (1997).
2. D. Oesterhelt and W. Stoeckenius, *Nature New Biol.* **233**, 149 (1971).
3. W. D. Hoff, K. H. Jung, J. L. Spudich, *Annu. Rev. Biophys. Biomol. Struct.* **26**, 223 (1997).
4. N. Grigorieff, T. A. Ceska, K. H. Downing, J. M. Baldwin, R. Henderson, *J. Mol. Biol.* **259**, 393 (1996).
5. J. K. Lanyi, *J. Struct. Biol.* **124**, 164 (1998).
6. J. A. Bieszke *et al.*, *Proc. Natl. Acad. Sci. U.S.A.* **96**, 8034 (1999).
7. J. A. Bieszke, E. N. Spudich, K. L. Scott, K. A. Borkovich, J. L. Spudich, *Biochemistry* **38**, 14138 (1999).
8. T. D. Mullins, T. B. Britcshgi, R. L. Krest, S. J. Giovannoni, *Limnol. Oceanogr.* **40**, 148 (1995).
9. O. Béjà *et al.*, *Environ. Microbiol.*, in press.
10. A subclone shotgun library was constructed from BAC clone 31A08, and subclones were sequenced in both directions on the MegaBACE 1000 capillary array electrophoresis DNA sequencing instrument (Molecular Dynamics, Sunnyvale, CA). The contiguous sequence was assembled with SEQUENCHER 3.1.1 software (Gene Codes, Ann Arbor, MI). The sequence of the proteorhodopsin-containing contig has been deposited in GenBank under accession number AF279106.
11. The protein most similar to proteorhodopsin was the sensory rhodopsin from *Natronomonas pharaonis* and bacteriorhodopsin from *Halobacterium halobium*, with a random expectation value of 2×10^{-10} and 30% identity in a 224–amino acid alignment and a random expectation value of 9×10^{-9} and 27% identity over 228 amino acids, respectively.
12. L. Aravind, R. L. Tatusov, Y. I. Wolf, D. R. Walker, E. V. Koonin, *Trends Genet.* **14**, 442 (1998).
13. W. F. Doolittle, *Science* **284**, 2124 (1999).
14. Considering differences in the ionic environment, sequence differences between archaeal and bacterial rhodopsins might be expected to accumulate at residues near the solvent interface. To understand the spatial distribution of these amino acid substitutions, a model of the proteorhodopsin was constructed using the known crystal structure of bacteriorhodopsin. The model was constructed by threading the proteorhodopsin sequence on the 1.55 Å resolution structure of bacteriorhodopsin [H. Luecke, B. Schobert, H. T. Richter, J. P. Cartailler, J. K. Lanyi, *J. Mol. Biol.* **291**, 899 (1999)]. This pairwise alignment was adjusted to minimize the Sippl mean force field energy [M. J. Sippl, *J. Mol. Biol.* **213**, 859 (1990)]. This was followed by model construction with PROMODII and energy minimization with the CHARMM force field. The structure was visualized with the Swiss PDB viewer [N. Guex and M. C. Peitsch, *Electrophoresis* **18**, 2714 (1997)]. In comparison to the most closely related archaeal sequences, the majority of the nonconservative substitutions resulted in changes in residue polarity and were typically localized to regions of solution contact (*19*). In contrast to archaeal rhodopsins, proteorhodopsin lacks a region between helix B and C that adopts an extended conformation and is in contact with solution on the extracellular surface.
15. Conserved amino acid residues include Lys^{231} (Lys^{216}), which forms the Schiff base with retinal; Arg^{94} (Arg^{82}); Asp^{97} (Asp^{85}); Thr^{101} (Thr^{89}); and Asp^{227} (Asp^{212}). The numbering begins with the NH_2-terminal residue of proteorhodopsin; the numbers of the corresponding residues in the well-characterized bacteriorhodopsin from *Halobacterium salinarum* are indicated in parentheses. Of these residues, Asp^{97} (Asp^{85}) is critical for proton transfer from the photoactivated retinal. Residue Asp^{227} (Asp^{212}) probably interacts with another conserved site, Tyr^{200} (Tyr^{185}), which contributes to the required environment for the proton conduit from the Schiff base [J. Heberle, *Biochim. Biophys. Acta* **1458**, 135 (2000)]. Arg^{94} (Arg^{82}) appears to regulate the process of proton release that occurs before the proton uptake from the cytoplasm [R. Govindjee *et al.*, *Biophys. J.* **71**, 1011 (1996)]. Thus, the essential steps of light-driven proton pumping by proteorhodopsin likely follow the same path as in the archaeal bacteriorhodopsins. Glu^{108} of proteorhodopsin corresponds to Asp^{96} of bacteriorhodopsin, the proton donor to the Schiff base in the reprotonation phase of the pumping cycle. The carboxylic acid residue in this position is shared by bacteriorhodopsins and proteorhodopsin, but not by sensory rhodopsins and halorhodopsins, which suggests mechanistic similarity between proteorhodopsin and bacteriorhodopsins in the proton uptake stage of their pumping cycles. A major difference between proteorhodopsin and bacteriorhodopsins is apparent in the pathway of proton release to the exterior of the cell. In bacteriorhodopsin, this step is largely mediated by two glutamates, Glu^{194} and Glu^{204} [L. S. Brown *et al.*, *J. Biol. Chem.* **270**, 27122 (1995); S. P. Balashov *et al.*, *Biochemistry* **36**, 8671 (1997)]. One or both of these residues are missing in other members of the prokaryotic rhodopsin family. Examination of the distribution of negatively charged residues on the external face of proteorhodopsin using a structural model (*14*) shows that Asp^{27}, Glu^{65}, Asp^{88}, Glu^{142}, and Asp^{212} are candidates for forming the proton path. Of these residues, Glu^{142} and Glu^{65} appear to be optimally positioned to act as the principal proton acceptors in the release process.
16. The 16*S* ribosomal RNA neighbor-joining tree was constructed on the basis of 1256 homologous positions by the "neighbor" program of the PHYLIP package [J. Felsenstein, *Methods Enzymol.* **266**, 418 (1996)]. DNA distances were calculated with the Kimura's 2-parameter method. The proteorhodopsin tree was constructed on the basis of the archaeal rhodopsin alignment used by Mukohata *et al.* [Y. Mukohata, K. Ihara, T. Tamura, Y. Sugiyama, *J. Biochem. (Tokyo)* **125**, 649 (1999)] and the neighbor-joining method as implemented in the neighbor program of the PHYLIP package. The numbers at forks indicate the percent of bootstrap replications (out of 1000) in which the given branching was observed. The least-square method (the Kitsch program of PHYLIP) and the maximum likelihood method (the Puzzle program) produced trees with essentially identical topologies, whereas the protein parsimony method (the Protpars program of PHYLIP) placed proteorhodopsin within the sensory rhodopsin cluster. The Yro/Hsp30 subfamilies sequences (*6*) were omitted from the phylogenetic analysis to avoid the effect of long branch attraction.
17. Proteorhodopsin was amplified from the 130-kb bacterioplankton BAC clone 31A08 by polymerase chain reaction (PCR), using the primers 5′-ACCATGGGTAAATTATTACTGATATTAGG-3′ and 5′-AGCATTAGAAGATTCTTTAACAGC-3′. The amplified fragment was cloned with the pBAD TOPO TA Cloning Kit (Invitrogen). The protein was cloned with its native signal sequence and included an addition of the V5 epitope and a polyhistidine tail in the COOH-terminus. The same PCR product in the opposite orientation was used as a negative control. The protein was expressed in the *E. coli* outer membrane protease-deficient strain UT5600 [M. E. Elish, J. R. Pierce, C. F. Earhart, *J. Gen. Microbiol.* **134**, 1355 (1988)] and induced with 0.2% arabinose for 3 hours. Membranes were prepared according to Shimono *et al.* [K. Shimono, M. Iwamoto, M. Sumi, N. Kamo, *FEBS Lett.* **420**, 54 (1997)] and resuspended in 50 mM tris-Cl (pH 8.0) and 5 mM $MgCl_2$. The absorbance spectrum was measured according to Bieszke *et al.* (*7*) in the presence of 10 μM all-*trans* retinal.
18. W. Stoeckenius, R. H. Lozier, R. A. Bogomolni, *Biochim. Biophys. Acta* **505**, 215 (1978).
19. O. Béjà *et al.*, data not shown.
20. Right-side-out membrane vesicles were prepared according to Kaback [H. R. Kaback, *Methods Enzymol.* **22**, 99 (1971)]. Membrane electrical potential was measured with the lipophilic cation TPP^+ by means

of rapid filtration [E. Prossnitz, A. Gee, G. F. Ames, *J. Biol. Chem.* **264**, 5006 (1989)] and was calculated according to Robertson *et al.* [D. E. Robertson, G. J. Kaczorowski, M. L. Garcia, H. R. Kaback, *Biochemistry* **19**, 5692 (1980)]. No energy sources other than light were added to the vesicles, and the experiments were conducted at room temperature.
21. R. A. Bogomolni *et al.*, *Proc. Natl. Acad. Sci. U.S.A.* **91**, 10188 (1994).
22. V. J. Yao and J. L. Spudich, *Proc. Natl. Acad. Sci. U.S.A.* **89**, 11915 (1992).
23. R. Seidel *et al.*, *Proc. Natl. Acad. Sci. U.S.A.* **92**, 3036 (1995).
24. N. R. Pace, *Science* **276**, 734 (1997).
25. J. A. Fuhrman, K. McCallum, A. A. Davis, *Appl. Environ. Microbiol.* **59**, 1294 (1993).
26. T. M. Schmidt, E. F. DeLong, N. R. Pace, *J. Bacteriol.* **173**, 4371 (1991).
27. M. T. Suzuki *et al.*, *Appl. Environ. Microbiol.* **63**, 983 (1997).
28. M. S. Rappe, P. F. Kemp, S. J. Giovannoni, *Limnol. Oceanogr.* **42**, 811 (1997).
29. S. G. Acinas, J. Anton, F. Rodriguez-Valera, *Appl. Environ. Microbiol.* **65**, 514 (1999).
30. M. T. Suzuki *et al.*, unpublished data.
31. H. Eilers, J. Pernthaler, F. O. Glockner, R. Amann, *Appl. Environ. Microbiol.* **66**, 3044 (2000).
32. J. G. Keunen, L. A. Robertson, O. H. Tuovinen, in *The Prokaryotes*, A. Balows, H. G. Truper, M. Dworkin, W. Harder, K. H. Schleifer, Eds. (Springer, Berlin, 1991), pp. 2638–2657.
33. Single-letter abbreviations for the amino acid residues are as follows: A, Ala; C, Cys; D, Asp; E, Glu; F, Phe; G, Gly; H, His; I, Ile; K, Lys; L, Leu; M, Met; N, Asn; P, Pro; Q, Gln; R, Arg; S, Ser; T, Thr; V, Val; W, Trp; and Y, Tyr.
34. J. Sasaki and J. L. Spudich, *Biophys. J.* **75**, 2435 (1998).
35. We thank C. M. Sakamoto for help with pH measurements and the captain and crew of the RV *Point Lobos* for sampling opportunities at sea. This work was supported in part by NSF grant OCE 0001619 (E.F.D.), by support provided to the Monterey Bay Aquarium Research Institute by the David and Lucile Packard Foundation, by NIH grants HG01775-02S1 (S.B.J.) and R01GM27750 (J.L.S.), and by a long-term postdoctoral fellowship to O.B. from the European Molecular Biology Organization.

9 May 2000; accepted 7 August 2000

REPORTS

Optically Induced Entanglement of Excitons in a Single Quantum Dot

Gang Chen,[1] N. H. Bonadeo,[1]* D. G. Steel,[1]† D. Gammon,[2] D. S. Katzer,[2] D. Park,[2] L. J. Sham[3]

Optically induced entanglement is identified by the spectrum of the phase-sensitive homodyne-detected coherent nonlinear optical response in a single gallium arsenide quantum dot. The electron-hole entanglement involves two magneto-excitonic states differing in transition energy and polarization. The strong coupling needed for entanglement is provided through the Coulomb interaction involving the electrons and holes. The result presents a first step toward the optical realization of quantum logic operations using two or more quantum dots.

Entanglement is one of the most spectacular peculiarities of quantum mechanics that contrast with classical physics (*1*). While it can occur between separate degrees of freedom of a single particle (*2*), only interparticle entanglement bears the properties of nonlocality that are essential for quantum information manipulation (*3*), such as teleportation, cryptography, and computation (*4*). Entangled states involving photons (*5*) or massive particles (*6–9*) have been produced by various experimental means. In addition, fundamental quantum logic gates and a number of quantum algorithms have also been demonstrated using these systems (*10–12*).

Recently, semiconductor quantum dot (QD) systems have been proposed as the basic building blocks for solid-state–based quantum logic devices due to their potential advantages, including the existence of an industrial base for semiconductor processing and the ease of integration with existing devices (*13–15*). The rapid technological advances seem to promise sophisticated engineering of the QD structures with the potential for the production of scalable coupled-QD systems (*16, 17*). However, neither entanglement nor any quantum logic operation has been realized in these systems.

We report the production and detection of an entangled state involving two excitonic states localized in a single GaAs QD, demonstrating an important first step toward the goal of entangling excitons confined to two or more semiconductor QDs. Single-QD exciton states are addressed with high spatial resolution using optical excitations that promote electrons from the heavy-hole levels of a single QD (with projected angular momentum of $\pm 3\hbar/2$) to the first excited electronic states (with projected angular momentum of $\pm\hbar/2$). An external static magnetic field is applied in the Faraday configuration to split both the hole and electron levels. It has been shown (*18*) that, despite the interacting electron nature of the semiconductor ground state, the low-lying state of a single electron and hole excitation is a well-defined single-particle state and that the exciton is a well-defined electron-hole pair state with only mutual attraction. All relevant energy levels and the two optically allowed circularly polarized (σ_+ and σ_-) transitions at frequencies ω_+ and ω_- are shown (Fig. 1A). Two mutually coherent laser fields, σ_+ polarized at frequency Ω_+ and σ_- at frequency Ω_-, respectively, excite these two transitions, producing the entangled state (Fig. 1B). In the excitonic picture, the total wavefunction can be written as

$$|\Psi\rangle = C_0|0\rangle + C_+|-1/2, +3/2\rangle + C_-|+1/2, -3/2\rangle \quad (1)$$

a nonfactorizable wavefunction involving the $|-1/2, +3/2\rangle$ and $|+1/2, -3/2\rangle$ excitons. Our notation for single-exciton states keeps track of the angular momentum of the excited electron and the hole left behind. The state $|0\rangle$ is the many-exciton vacuum (crystal ground state), $|-1/2, +3/2\rangle$ represents the σ_+ (or spin-up) exciton state where an electron in the $-3\hbar/2$ level is promoted to the $-\hbar/2$ level (through a σ_+ transition), leaving a hole with angular momentum of $+3\hbar/2$. Similarly, $|+1/2, -3/2\rangle$ represents the σ_- (or spin-down) exciton state.

In order to optically excite a nonfactorizable wavefunction and produce an entangled state of two quantum systems, it is known that a strong coupling is required (*19*). In the case of two excitons in a quantum dot, the coupling is due to the strong Coulomb interaction (*20*). This is best seen from the four-level diagram (Fig. 1C) in the two-exciton basis (*21*). While leaving the exciton vacuum and the single-exciton states unaffected, it leads to an energy shift of the two-exciton level $|-1/2, +3/2, +1/2, -3/2\rangle$ (represented by t in the absence of this interaction), which becomes either a bound biexciton state (denoted by b) or a scattering state of two excitons (denoted by s). The photoluminescence of the biexciton state for similar dots in this study have been reported in (*22*). Because of the narrow-band excitation used to excite the single-exciton states, the b (or s) state is out of resonance and therefore does not contribute to

[1]Harrison M. Randall Laboratory of Physics, University of Michigan, Ann Arbor, MI 48109–1120, USA. [2]The Naval Research Laboratory, Washington, DC 20375, USA. [3]Department of Physics, University of California San Diego, La Jolla, CA 92093–0319, USA.

*Present address: Bell Laboratories, 101 Crawfords Corner Road, Holmdel, NJ 07733, USA.
†To whom correspondence should be addressed. E-mail: dst@eecs.umich.edu